

PARAMETER IDENTIFICATION AND SENSITIVITY ANALYSIS FOR ZERO-DIMENSIONAL MULTI-PHYSICS LITHIUM-SULFUR BATTERY MODELS

Chu Xu, Timothy Cleary, Guoxing Li, Donghai Wang and Hosam K. Fathy *

ABSTRACT

This paper examines the problem of estimating the parameters of a Lithium-Sulfur (LiS) battery from experimental cycling data. LiS batteries are attractive compared to traditional Lithium-Ion batteries, thanks largely to their potential to provide higher energy densities. The literature presents a number of different LiS battery models, with different fidelities and complexities. This includes both higher-fidelity diffusion-reaction models as well as “zero-dimensional” models that neglect diffusion dynamics while capturing the physics of the underlying reduction-oxidation reactions. The paper focuses on zero-dimensional LiS battery models, and develops four such models from the literature, reflecting different choices of which redox reactions to model. There is a growing need for using experimental cycling datasets to both parameterize these models and compare their fidelities. To address this need, we fabricated LiS coin cells and performed charge/discharge cycling tests on these cells. In parallel, we analyzed the sensitivity of simulated LiS battery charge/discharge characteristics to underlying model parameters. Using this sensitivity analysis, we selected a subset of model parameters for identification, and estimated these parameters for all four LiS battery models from cycling data, thereby arriving at a consistent experimental comparison and assessment of these models’ respective fidelities.

NOMENCLATURE

i	Species index
j	Reaction index
q	Number of species
p	Number of reactions
m_i	Mass of species i [g]
m_{S_p}	Mass of precipitated sulfur [g]
i_j	Current generated by reaction j [A]
I	Input (discharge) current [A]
E_j	Reduction potential for reaction j [V]
η_j	Overpotential for reaction j [V]
V	Output voltage across the cell [V]
ε	Relative porosity
a_v	Active reaction area [m^2]
n_{S_i}	Number of sulfur atoms in species i
n_j	Number of electrons exchanged in reaction j
M_S	Molar mass of a sulfur atom [g/mol]
F	Faraday’s constant [C/mol]
R	Gas constant [J/(K mol)]
T	Room temperature 298 [K]
v	Cell volume [L]
S_{sat}	Saturation mass of S^{2-} [g]
$s_{i,j}$	Stoichiometric coefficients
m_i^0	Initial mass of species i [g]
E_j^0	Standard reduction potentials [V]
i_j^0	Exchange current density [A/m^2]
a_v^0	Initial active reaction area [m^2]
γ	Power of the relative porosity
ω	Relative porosity change rate constant [1/g]
k_p	Precipitation rate constant [1/(g s)]

*Chu Xu (chuxu88@umd.edu) is a graduate student and Hosam K. Fathy (hfathy@umd.edu, the corresponding author) is a professor of Mechanical Engineering at the University of Maryland, College Park, MD, 27042. Timothy Cleary (tdc142@psu.edu) is a graduate student of Mechanical Engineering at Penn State University. Guoxing Li (gxli@sdu.edu.cn) is a professor at The Science Center for Material Creation and Energy Conversion, Institute of Frontier and Interdisciplinary Science, Shandong University, Qingdao, China. Donghai Wang (dwang@psu.edu) is a professor of Mechanical Engineering at Penn State University.

INTRODUCTION

As the performance of Lithium-ion (Li-ion) batteries approaches its practical limit (up to 500 Wh/kg), researchers are actively seeking alternative, higher energy density solutions. The Lithium-Sulfur (LiS) chemistry is one such alternative solution. It has attracted significant attention from the scientific community for at least four reasons. First, the LiS chemistry offers very attractive theoretical limits for specific capacity (1672 Ah/kg) and specific energy (2600 Wh/kg). This can furnish lighter batteries for the same energy capacity. Prototype Lis cells, for instance, have achieved specific energies around 700 Wh/kg [1]. Second, LiS batteries have the potential to offer a range of operating temperatures from -40 to 60 Celsius [2]. This is especially beneficial for low temperature applications. Third, phenomena such as precipitation and the internal charge shuttle effect provide LiS batteries with some degree of intrinsic overcharge protection [3, 4], thereby making them less vulnerable to catastrophic thermal events compared to their Li-ion counterparts. Fourth, the use of sulfur instead of other materials, including rare earth metals, makes LiS batteries quite appealing compared to Li-ion batteries in terms of factors such as production cost and environmental footprint [5].

The above advantages of the LiS chemistry come with some costs. The LiS chemistry suffers from low cycle life and relatively high self-discharge rates [6, 7]. Effort has been made to improve these batteries' performance from the electrochemical/material perspective [8]. This paper is part of a parallel effort to improve LiS battery performance and longevity through modeling, estimation, and, ultimately, health-conscious control. The paper focuses specifically on the problem of parameterizing LiS battery models from experimental data: a critical first step towards model-based control.

The literature already presents a number of LiS battery models that can be used for parameter estimation and model-based control. These models fall on a spectrum of fidelity and complexity levels. Equivalent circuit models (ECMs) of LiS batteries sit at one end of this spectrum. They typically combine empirical open-circuit voltage maps with (often charge- and temperature-dependent) resistor-capacitor circuits [9–12]. Typical uses of such simple models include online state of charge estimation [13–15]. At the other end of the spectrum, one finds multiphysics-based models of the reduction-oxidation, diffusion, precipitation, and self-discharge dynamics in LiS batteries. These are typically partial differential algebraic equation (PDAE) models of coupled diffusion-reaction dynamics [16–21]. They have the advantage of providing higher-fidelity representations of the underlying battery physics, at the expense of high complexity. “Zero-dimensional” (0D) models provide an important middle ground between these two modeling extremes. They neglect the diffusion of species inside LiS batteries, but use the laws of electrochemistry to model the underlying battery reactions. This approach results in lower-order models with

fewer parameters to identify and reduced computational complexity. Simplified two-reaction and multi-reaction 0D models introduced in [22] and [23] are able to capture the main features of battery voltage response during discharge. The computational complexity of a zero-dimensional LiS battery model depends on the specific choice of which reactions to model, and which to ignore. One potential approach for making this choice is to compare the fidelity with which different zero-dimensional models can fit a given experimental charge/discharge dataset. Such an exercise is appealing because it can furnish both: (i) a systematic comparison between different battery models using the same dataset plus (ii) an experimental parameterization of different zero-dimensional LiS battery models. To the best of the authors' knowledge, both of these contributions remain relatively unexplored in the literature. The overarching goal of this work is to address this research gap.

Starting from previous work on 0D LiS models, this work goes one step further to analyze different 0D models capturing different underlying redox reactions. The goal is to answer the following questions: (i) How does each reaction influence the discharge voltage curve in a 0D model? (ii) Do all the model parameters have a significant impact on the discharge voltage curve? Is it necessary to identify them all? (iii) How well can one perform parameter identification experimentally based on the 0D models? The ultimate goal is to provide guidance on the choice of which reactions to model for future applications, such as SOC/SOH estimation. The remainder of this paper addresses these questions, and is organized as follows. Firstly, the authors describe the zero dimensional model structure adopted from [22, 23], combined with the reduction reactions considered in each model. The following section provides a simulation study illustrating the effects of different reactions on the discharge voltage performance. Then, the authors perform a parameter sensitivity study to provide guidance which parameters are critical to identify from cycling experiments. Section V presents the parameter identification results using experimental data. Finally, section VI summarizes this paper's conclusions.

ZERO-DIMENSIONAL MULTI-PHYSICS MODELS

This section describes the 0D reaction models used for subsequent analysis in the paper. The models build on two existing bodies of work in the literature. First, research by Zhang *et al.* [23] develops a lumped model describing the dynamics of dissolved species concentrations and cathode material porosity in LiS batteries. Moreover, this model includes the full reduction reaction chain and the effective electrolyte resistance. Second, research by Marinescu *et al.* [22] introduces another 0D model taking into account the dynamic evolution of different species' masses as well as the shuttle effect. The model simplifies the chain of sulfur reduction reactions into two steps. We adopt/combine the underlying structures of the above two mod-

TABLE 1. REDUCTION REACTIONS CONSIDERED IN THE MODELS

Models	Model #1	Model #2	Model #3	Model #4
Reduction Reactions	$\frac{1}{4}S_8 + e^- \rightleftharpoons \frac{1}{2}S_4^{2-}$	$\frac{3}{8}S_8 + e^- \rightleftharpoons \frac{1}{2}S_6^{2-}$	$\frac{1}{2}S_8 + e^- \rightleftharpoons \frac{1}{2}S_8^{2-}$	$\frac{1}{2}S_8 + e^- \rightleftharpoons \frac{1}{2}S_8^{2-}$
	$\frac{1}{6}S_4^{2-} + e^- \rightleftharpoons \frac{2}{3}S^{2-}$	$S_6^{2-} + e^- \rightleftharpoons \frac{3}{2}S_4^{2-}$	$\frac{3}{2}S_8^{2-} + e^- \rightleftharpoons 2S_6^{2-}$	$\frac{3}{2}S_8^{2-} + e^- \rightleftharpoons 2S_6^{2-}$
		$\frac{1}{6}S_4^{2-} + e^- \rightleftharpoons \frac{2}{3}S^{2-}$	$S_6^{2-} + e^- \rightleftharpoons \frac{3}{2}S_4^{2-}$	$S_6^{2-} + e^- \rightleftharpoons \frac{3}{2}S_4^{2-}$
			$\frac{1}{6}S_4^{2-} + e^- \rightleftharpoons \frac{2}{3}S^{2-}$	$\frac{1}{2}S_4^{2-} + e^- \rightleftharpoons S_2^{2-}$
				$\frac{1}{2}S_2^{2-} + e^- \rightleftharpoons S^{2-}$
Dissolved Sulfur Species	S_8, S_4^{2-}, S^{2-}	$S_8, S_6^{2-}, S_4^{2-}, S^{2-}$	$S_8, S_8^{2-}, S_6^{2-}, S_4^{2-}, S^{2-}$	$S_8, S_8^{2-}, S_6^{2-}, S_4^{2-}, S_2^{2-}, S^{2-}$

els, and expand these models to capture the dynamics of different sets of reduction reactions. The end result is a set of four zero-dimensional models. The simplest model covers the minimum set of reduction reactions modeled in the literature, whereas the most complex model covers the full set of sulfur reduction reactions in LiS batteries. The reactions considered in each model are listed in Table 1.

A typical LiS battery discharge voltage curve consists of high and low plateaus. In the high plateau region, the active material, S_8 , in the cathode accepts electrons to produce the polysulfide, S_x^{2-} (x can be 8, 6, 4). Further polysulfide reduction takes place in the lower voltage plateau region [24]. In parallel, lithium is oxidized in the anode to furnish lithium ions. In this work, the authors adopt the following modeling assumptions from the literature: (i) there is an unlimited amount of lithium supply in the cell with a negligible overpotential on the anode side, as in [17]; (ii) the shuttle effect of polysulfides is not included due to this paper's focus on the voltage performance instead of capacity fade [23]; and (iii) only the lowest polysulfide's precipitation reaction ($2Li^+ + S^{2-} \rightleftharpoons Li_2S \downarrow$) is modeled [22,23].

Since the model is zero-dimensional, there exists no mass transport due to diffusion/migration. The only dynamics changing the masses of the dissolved species are the electrochemical reaction and precipitation. These dynamics lead to the time-evolution relations for the masses of various sulfur species and the porosity of the cathode material, which act as the state variables in the model. Below is the resulting differential algebraic equation (DAE) model (assuming discharge) including both state equations and algebraic constraints. Descriptions of the model's variables and parameters are included in the paper's nomenclature section.

State Equations:

$$\dot{m}_i = \sum_j \frac{n_{S_i} M_s}{n_j F} s_{i,j} i_j, \quad \text{for } i = 1, \dots, q-1 \quad (1)$$

$$\dot{m}_q = \frac{n_{S_q} M_s}{n_p F} s_{q,p} i_p - \dot{m}_{S_p} \quad (2)$$

$$\dot{m}_{S_p} = k_p m_{S_p} (m_q - S_{sat}) \quad (3)$$

$$\dot{\varepsilon} = -\omega m_{S_p} \quad (4)$$

Constraints:

$$E_j = E_j^0 - \frac{RT}{n_j F} \sum_i s_{i,j} \ln\left(\frac{m_i}{n_{S_i} M_s v}\right) \quad (5)$$

$$i_j = -a_v i_j^0 \left\{ \prod_i \left(\frac{m_i}{m_i^0}\right)^{s_{i,j}} e^{\left(\frac{F}{2RT}\eta_j\right)} - \prod_i \left(\frac{m_i}{m_i^0}\right)^{-s_{i,j}} e^{\left(-\frac{F}{2RT}\eta_j\right)} \right\} \quad (6)$$

$$a_v = a_v^0 \varepsilon^\gamma \quad (7)$$

$$I = \sum_j i_j \quad (8)$$

$$V = \eta_j + E_j \quad (9)$$

The rates of mass change for higher-order dissolved sulfide species are governed by Eqn. 1. For species S^{2-} , one needs to consider its mass generation from the last reduction reaction and

its mass loss due to precipitation. The nucleation and growth phenomenon is described by Eqn. 3 [22]. The rate of change of the mass of the precipitate is driven by the precipitate mass. This reflects the fact that the existing precipitate serves as a nucleus for further precipitation/growth, as long as the mass in the electrolyte is above a given saturation mass.

Relative porosity is one of the state variables in the model. This variable equals the current porosity of the cathode material divided by initial porosity, and has a direct effect on the active reaction area, as shown in Eqn. 7 [16]. When the porosity decreases to zero, all the reactants are blocked by the precipitate from the cathode material surface. This can be one of the indicators of the cell's full discharge, another full discharge scenario being the reduction of all polysulfides to S^{2-} . As the cell approaches complete coverage of the cathode ($\epsilon \rightarrow 0$), larger overpotentials (η_j) are needed for the same current. This provides one explanation of the low measured voltage at the end of LiS battery discharge.

The reduction potential of each reaction is given by the Nerst equation (Eqn. 5), assuming that E_j^0 is the equilibrium potential when the concentration of the dissolved species in reaction j is 1 mol/L [23]. The current generated by the corresponding reduction reaction is described by the Butler–Volmer equation (Eqn. 6). All these currents sum to the only input variable, namely, the external discharge current I . The voltage measured across the battery equals the summation of the overpotential and the reduction potential of each reaction, as shown in Eqn. 9.

VOLTAGE RESPONSES FOR DIFFERENT REACTION CHAINS

In the literature, there exists different simplifications of the reaction chain on the cathode side, such as the two-step reduction $S_8 \rightarrow S_4^{2-} \rightarrow S^{2-}$ [25] and the four-step reduction $S_8 \rightarrow S_8^{2-} \rightarrow S_6^{2-} \rightarrow S_4^{2-} \rightarrow S^{2-}$ [19]. Different LiS battery models, capturing different representations of the overall reaction chain, are built to suit the focus areas of different research studies. In this section, the authors compare the simulated voltage outputs of the models in Table 1 and analyze each reaction's influence on the different features of the discharge voltage curve. We use OpenModelica to build and simulate the models with the key parameter values listed in Table 2. The simulated discharge voltage-capacity curves are compared in Fig. 1.

The main observations from the above simulation results are as follows. First, all the reaction models provide similar specific capacity values, approximately 1675 mAh/g, matching the theoretical specific capacity value in [8]. This implies that all four models are potentially useful for capacity studies. Second, the intermediate reactions associated with the high plateau can influence this plateau's shape and duration. Specifically, when the high plateau reaction is simplified to only $S_8 \rightarrow S_4^{2-}$ in Model #1, the voltage curve shows a relatively longer duration for this

TABLE 2. PARAMETER VALUES IN SIMULATIONS

Notations	Values	Units
Model #1		
E_j^0	2.40, 2.10	V
i_j^0	2.00, 0.02	A/m^2
Model #2		
E_j^0	2.40, 2.30, 2.10	V
i_j^0	2.00, 0.02, 0.02	A/m^2
Model #3		
E_j^0	2.46, 2.38, 2.30, 2.10	V
i_j^0	2.00, 0.02, 0.02, 0.02	A/m^2
Model #4		
E_j^0	2.46, 2.38, 2.30, 2.15, 1.98	V
i_j^0	2.00, 0.02, 0.02, 0.02, 0.02	A/m^2
For all the models		
v	0.0114	L
S_{sat}	0.0001	g
a_v^0	1	m^2
γ	1.5	-
ω	0.1	$1/g$
k_p	22	$1/(g s)$

plateau. Moreover, this high plateau ends with a dramatic, almost vertical voltage drop. The same observation is presented in [18]. This drop can be explained by the potential dynamics given by Eqn. 10. At the end of the reaction, the mass of the reactant approaches zero, while the rate of change of this mass maintains a relatively stable value due to the fact that i_j still needs to meet the external discharge current value. This results in $\dot{E}_j \rightarrow -\infty$. Hence, the measured voltage V exhibits an almost vertical drop. When intermediate reactions are added between S_8 and S_4^{2-} , a milder slope emerges with the dip between the plateaus occurring at higher voltages. Also, the more reactions one adds to the model, the longer the shallow portion of the high-plateau region prevails.

$$\dot{E}_j = -\frac{RTM_sv}{n_jF} \sum_i s_{i,j} n_{S_i} \frac{\dot{m}_i}{m_i} \quad (10)$$

This analysis provides the characteristics of the voltage

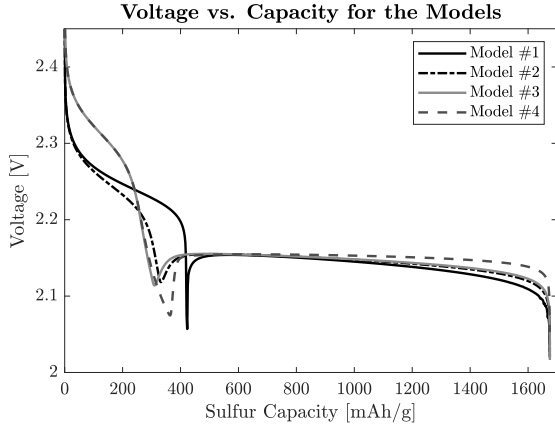


FIGURE 1. DISCHARGING VOLTAGES VS. SULFUR CAPACITY FOR THE REACTION MODELS

curve considering different reactions. The bottom line is that simplified representations of the reduction reactions are reasonable in terms of one's ability to capture theoretical specific capacity, but the influence on the voltage features is not negligible. One needs to choose the reactions carefully based on the purpose of the given application. For example, studies focused on the capacity fade may choose simpler models, while SOC estimation may require more complicated reaction models due to the accuracy needed in capturing the characteristics of output voltage.

PARAMETER SENSITIVITY ANALYSIS

One can broadly categorize the parameters of the above models into two groups. The first group includes parameters that are known *a priori*, such as Faraday's constant, the gas constant, standard temperature, molar mass, the number of electrons transferred in each reaction, etc. The second group contains unknowns such as the standard potentials, exchange current densities, the initial masses of the dissolved species, and precipitation-relevant parameters (i.e., the morphology parameters γ , ω , and precipitation rate). Increasing the number of reactions and species considered in the model increases the number of unknown parameters. Hence, the difficulty of parameterization increases. In this section, the authors analyze the sensitivity of the 0D model's output to the underlying parameters in order to better understand which parameters are important to identify.

Instead of using a theoretical parameter sensitivity approach [26], this work applies a similar analysis method to the work presented in [27–29] for a 1D LiS battery model. Specifically, we choose one parameter each time and investigate the voltage performance changes due to variations in this parameter while keeping the other parameters constant. This way, one can analyze the behavior of the model with respect to different situations and find a parameterization range for the parameters. This parameter

sensitivity analysis is performed on all the models presented in Table 1. Since the results show consistency for all the models, the full reaction model (Model #4) is chosen as a representative to show the results and discussions.

Intuitively, changing the parameters governing a particular reaction will change the model's performance during the time period when that reaction dominates. For example, if a phenomenon mainly emerges during low plateau, such as precipitation, changing the parameters describing that phenomenon affects the characteristics of the low plateau only, and vice versa for the high plateau.

Sensitivity to Standard Potential E_j^0

Fig 2 presents the results of analyzing the sensitivity of Model #4 to parameter E_j^0 . One can see the relative dominance of different reactions by observing the corresponding changes in the voltage curve. In Model #4, reaction $S_8 \rightarrow S_8^{2-}$ has a dominant influence on the high plateau voltage level. Reaction $S_6^{2-} \rightarrow S_4^{2-}$ has a strong effect on the "ending slope" of the high plateau and the dip point between the two plateaus, while slightly changing the low plateau voltage level. The last two reactions occur during the low plateau region, and therefore both of the corresponding standard potentials influence the voltage curve dramatically.

Sensitivity to Exchange Current Density i_j^0

The sensitivity analysis for i_j^0 is shown in Fig. 3. One can observe minor changes in the voltage curve within the the chosen range of i_j^0 . The exchange current densities of the middle reactions have negligible impacts on voltage, as the voltages curves are on top of each other. Compared to E_j^0 , which influences the voltage V through variable E_j , the parameter i_j^0 effects the overpotential η_j through an exponential function. On the one hand, this shows that E_j^0 and i_j^0 have similar effects on voltage, and highlights the challenge of identifying both i_j^0 and E_j^0 simultaneously from experimental data. On the other hand, bigger variations in i_j^0 produce smaller changes in the voltage curve compared to E_j^0 , which suggests the exchange current density has less impact on the model's voltage performance.

Sensitivity to Precipitation-Related Parameters

Four parameters essentially govern the precipitation phenomenon, namely, the saturation mass of dissolved S^{2-} , the precipitation rate k_p , and the morphology parameters of the relative porosity of the cathode γ and ω . The variations of each parameter produce changes in the low plateau region without influencing high plateau voltages, as shown in Fig. 4. When the saturation mass increases, more S^{2-} is dissolved in the electrolyte, reducing the potential of the reaction $S_x^{2-} \rightarrow S^{2-}$, hence providing a lower voltage across the battery. The precipitation rate k_p and morphology parameter γ determine the flatness of beginning and end

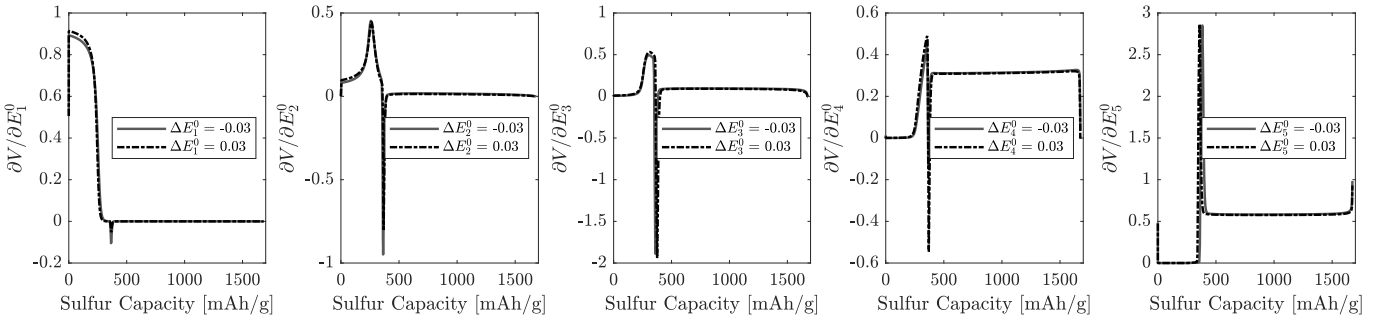


FIGURE 2. SENSITIVITY ANALYSIS OF E_j^0 FOR MODEL #4

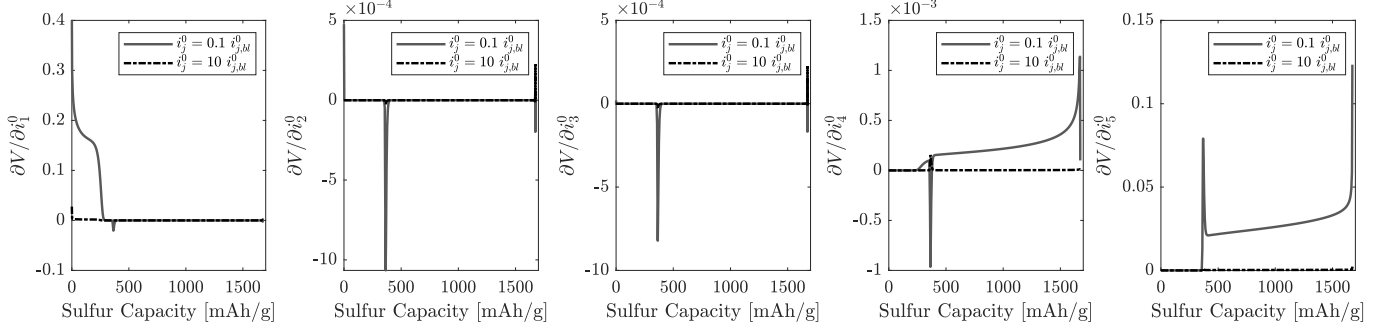


FIGURE 3. SENSITIVITY ANALYSIS OF i_j^0 FOR MODEL #4

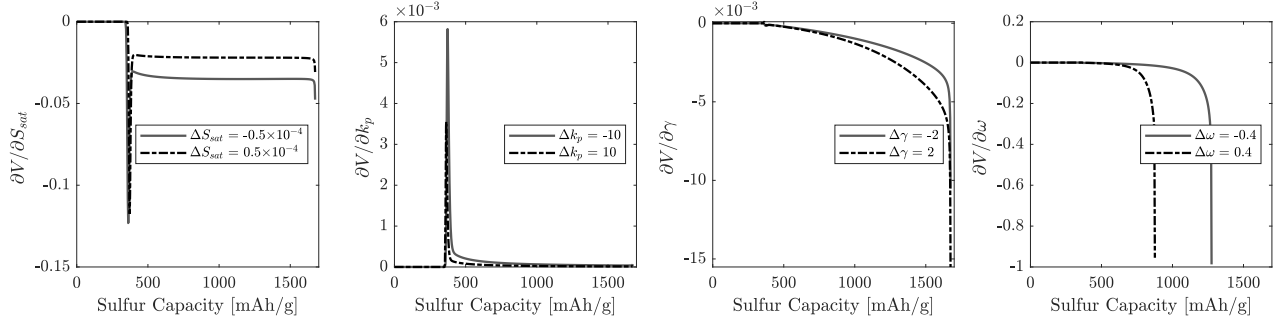


FIGURE 4. SENSITIVITY ANALYSIS OF PRECIPITATION RELEVANT PARAMETERS FOR MODEL #4

region of the low plateau. Bigger values of k_p and smaller values of γ provide a flatter low plateau. The parameter ω is the only parameter dramatically affecting the capacity of S_8 . With the increase in the rate of change of relative porosity, the discharge process can terminate earlier because of the resulting paucity of active reaction area inside the cathode material.

Sensitivity to Initial Mass of Dissolved S_8

The authors assume that all the active sulfur is dissolved into the electrolyte at the beginning of discharge. The mass of the dissolved S_8 is the main factor determining the total amount of active material inside the battery, and the initial masses of

other species at the beginning of discharge are comparatively very small. Here we only perform sensitivity analysis with respect to the initial mass of dissolved S_8 with a variation range of 2-4 grams. This has negligible impact on the voltage curve and specific capacity, as shown in Fig. 5. However, one must note that the voltage curve difference emerges when plotting the voltage with respect to time instead of specific sulfur capacity. Hence the dip point between the two plateaus changes markedly with respect to time.

From the above analysis, we have the following conclusions to guide parameter identification: (i) Although both E_j^0 and i_j^0 affect the voltage curve, V is more sensitive to E_j^0 . (ii) In the

set of parameters relevant to precipitation, correctly capturing the values ω and γ is more essential for capturing the shape of the low plateau. (iii) The initial mass of dissolved S_8 influences the timing of the dip point between the high and low plateaus. Hence, in the parameter identification study, the authors focus on parameters E_j^0 , γ , ω , and $m_{S_8}^0$, with all the other parameters treated as known constants.

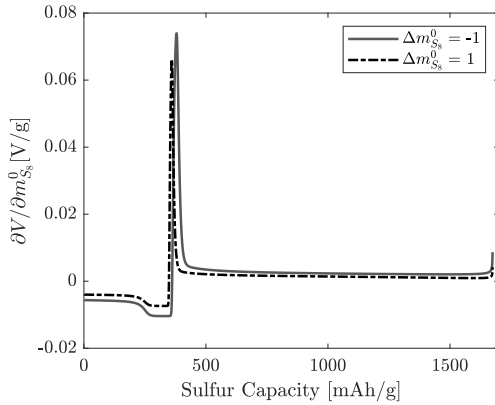


FIGURE 5. SENSITIVITY ANALYSIS OF INITIAL MASS OF DISSOLVED S_8 FOR MODEL #4

PARAMETER IDENTIFICATION RESULTS

It is difficult to systematically compare multiple models of LiS battery dynamics without fitting all of them to the underlying experimental data first. This section presents a parameterization study focusing on the proposed four reaction models. The authors obtain the test data through discharging a laboratory-made coin cell prototype.

Coin Cell Fabrication and Discharging Experiments

We fabricated a 2016-type coin cell using the recipe in [30]. The cathode material consisted of a C/S composite with 70 wt% sulfur, KB EC60JD to form a conductive framework, and PVDF dissolved in NMP as a binder. A lithium chip with 0.6 mm thickness served as the anode. The electrolyte used here was 1M $LiTFSI$ and 4 wt% $LiNO_3$ in the dioxolane/dimethoxylethane mixture (DOL/DME = 1:1, V/V). The sulfur loading of the cell was calculated as 0.521 mg. A constant discharge current of 0.03 mA was applied in the experiment to obtain the discharge voltage curve. Testing was conducted at room temperature, using ARBIN battery test equipment with special attention given to the accuracy of current control. In particular, a separate capacitor charge/discharge test was used for estimating the bias in the cycler's current measurement, and this bias was subtracted from

this paper's LiS battery cycling data.

Scaling From Model to Prototype Using Similitude

One caveat appears when we implement the experimentally-measured LiS cell current into the simulation model, namely, the need to scale the simulation model to match the physical sizing of the LiS coin cell used in this study. Here we use the idea of similitude to scale the relative variables/parameters from the model to the prototype. For all the fundamental dimensions in the model (i.e. time, mass, charge, length and temperature), charge is scaled by a given value μ , and we want to find the scaling factor of mass and length, with the other dimensions unchanged. Then the input current is scaled by μ due to the fact that time is unscaled. The relationship between the model and prototype input is shown in Eqn. 11 and applies to i_j as well. The subscript *mod* and *pro* represent model and prototype correspondingly.

$$I_{mod} = \mu I_{pro} \quad (11)$$

From Eqn. 1, we derive the scale on mass as below:

$$\frac{\dot{m}_{i,mod}}{\sum_j \frac{n_{S_i}}{n_j} s_{i,j} i_{j,mod}} = \frac{\dot{m}_{i,pro}}{\sum_j \frac{n_{S_i}}{n_j} s_{i,j} i_{j,pro}} \quad (12)$$

where other parameters are independent of mass and charge, except for \dot{m}_i and i_j . Hence, we have

$$m_{mod} = \mu m_{pro} \quad (13)$$

Using the same logic, we can derive the scale on length as $\mu^{\frac{1}{3}}$ from Eqn. 6, then the scale factors on parameters a_v , v , i_j^0 , ω , k_p are $\mu^{\frac{2}{3}}$, μ , $\mu^{\frac{1}{3}}$, $\frac{1}{\mu}$ and $\frac{1}{\mu}$. In the following parameterization simulation, the authors use 1A as the simulated model's input current with the corresponding μ being 3.33×10^4 . This value of μ scales the simulation model down to match the true scale of the fabricated laboratory coin cell.

Optimization Problem Formulation

The parameter identification study uses the least-squares method based on the above 0D reaction models. The least-squares method estimates parameters by minimizing the squared discrepancies between observed data and the expected values. With the models' highly nonlinear structure, one can use general optimization algorithms to locate the global optimal solution as the best estimated parameters. The authors choose the particle swarm optimization algorithm [31] to solve the resulting nonlinear least squares problem. The goal is to identify the parameter vector $\hat{\theta}$ by solving the least squares problem shown below:

TABLE 3. Parameter Identification Results

Model	Value	Units
Model #1		
E_j^0	2.4534, 2.0900	V
γ	0.3163	-
ω	0.5079	1/g
$m_{S_8,mod}^0$	2.0007	g
$m_{S_8,pro}^0$	0.0600	mg
Model #2		
E_j^0	2.4640, 2.3601, 2.0731	V
γ	0.4368	-
ω	0.5699	1/g
$m_{S_8,mod}^0$	2.6297	g
$m_{S_8,pro}^0$	0.0789	mg
Model #3		
E_j^0	2.4673, 2.3742, 2.3420, 2.0693	V
γ	0.4832	-
ω	0.6133	1/g
$m_{S_8,mod}^0$	3.0377	g
$m_{S_8,pro}^0$	0.0911	mg
Model #4		
E_j^0	2.4672, 2.3104, 2.2079, 2.0944, 1.9716	V
γ	0.9598	-
ω	0.6496	1/g
$m_{S_8,mod}^0$	3.5234	g
$m_{S_8,pro}^0$	0.1057	mg

$$\min_{\hat{\theta}} J = \sum_{k=1}^{N_{min}} (\hat{V}_k - V_{m,k})^2 + \alpha(\hat{T} - T)^2 \quad (14)$$

$$\text{where : } \boldsymbol{\theta} = [E_j^0, \gamma, \omega, m_{S_8}^0]^T, N_{min} = \min\{N, \hat{N}\} \quad (15)$$

subject to the dynamics of the system from Eqn. 1 to 9. In this problem formulation, \hat{V}_k and $V_{m,k}$ represent the estimated and measured output voltages at time step k ; \hat{T} and T are the final times of the simulation and experiment; and the weight α reflects the importance of minimizing the difference between the simulated and experimental discharge durations.

Results and Discussion

The identification results are listed in Table 3, with the corresponding estimated voltage shown in Fig. 6. The identified parameters for all the models are able to fit the experimental data in terms of the total discharging time. The objective function values corresponding to the best estimated parameters for the models are shown in Fig. 7. Interestingly, Model #3 performs the best fit with a minimum objective function value among all the models. The over-simplification of reactions in Model #1 leads to failure in capturing the slope of the voltage in the high plateau region. In contrast, the full reaction Model #4 does not provide a good fit in the middle region where the precipitation phenomenon emerges.

Another observation pertains to the simulation time needed for one discharge cycle, as shown in Fig. 8. Intuitively, the computational complexity of the models increases with the number of included reduction reactions. However, the execution time increases from Model #1 to Model #3 are minor, whereas the increase from Model #3 to Model #4 is quite dramatic. The full reaction model takes longer to simulate one discharge cycle in OpenModelica due to the model's complexity. One can conclude the best fit for further control application is Model #3. It provides the least discrepancy between the experimental data and simulation results, without excessive computational cost.

CONCLUSIONS

This paper performs parameter sensitivity analysis and identification for a variety of zero-dimensional multi-physics LiS battery models. We provide the answer of the questions listed in Introduction here: (i) The intermediate reactions between S_8 and S_4^{2-} add slope to the second half of the high plateau, while the reactions between S_4^{2-} and S^{2-} prolong the flat portion of this plateau and deepen the inter-plateau voltage dip. (ii) Sensitivity analysis provides guidance on the final choice of to-be-identified

parameters as E_j^0 (the voltage level), γ (the low plateau slope), ω (the low plateau duration) and $m_{S_8}^0$ (the dip location). (iii) Taking into account the intermediate reactions affecting the high plateau, the estimated voltage curve fits well with the experimental data except the beginning of discharge. Finally, taking into account the importance of balancing parameter identification performance versus execution time, the authors recommend Model #3 as the best model for use in future control oriented applications under this model structure.

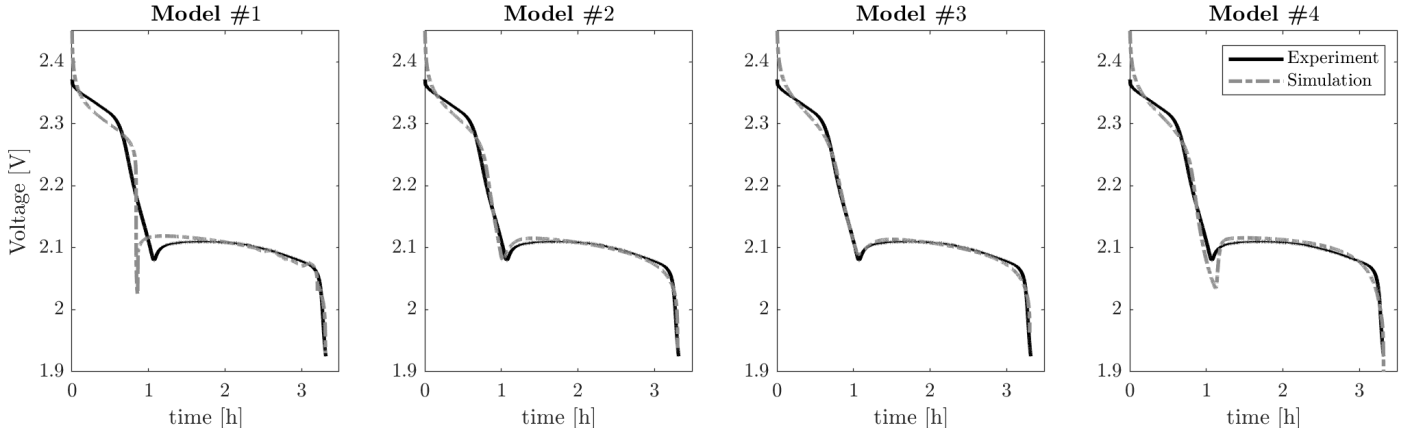


FIGURE 6. DISCHARGING VOLTAGE COMPARISON BETWEEN EXPERIMENT AND SIMULATION USING IDENTIFIED PARAMETERS FOR ALL THE MODELS

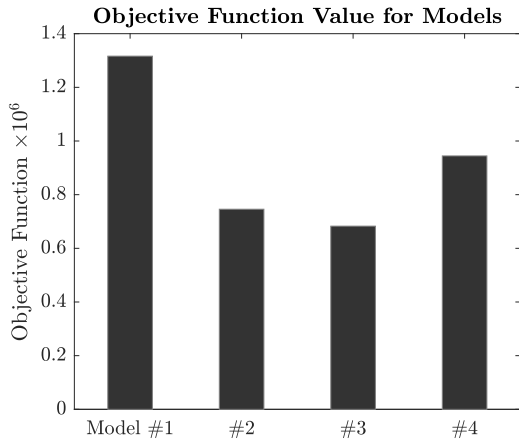


FIGURE 7. OBJECTIVE FUNCTION VALUES FOR THE MODELS

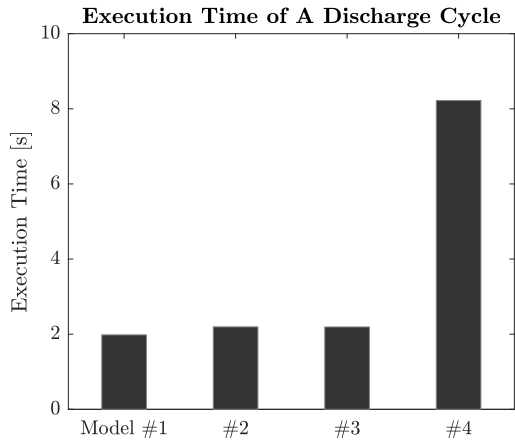


FIGURE 8. EXECUTION TIME OF ONE DISCHARGE CYCLE FOR THE MODELS

ACKNOWLEDGMENT

This work is funded by National Science Foundation Grant 1351146. The authors gratefully acknowledge this support. Any opinions, findings, and conclusions or recommendations expressed in this material are those of the authors and do not necessarily reflect the views of the National Science Foundation.

REFERENCES

- [1] Yanin, H., and Peled, E., 1983. "Low-rate lithium/sulfur organic battery". In Proc.-Electrochem. Soc.;(United States), Vol. 84, Department of Chemistry, Tel-Aviv University, Tel-Aviv.
- [2] Huang, J.-Q., Liu, X.-F., Zhang, Q., Chen, C.-M., Zhao, M.-Q., Zhang, S.-M., Zhu, W., Qian, W.-Z., and Wei, F., 2013. "Entrapment of sulfur in hierarchical porous

graphene for lithium–sulfur batteries with high rate performance from- 40 to 60 c". *Nano Energy*, 2(2), pp. 314–321.

- [3] Hunt, I. A., Patel, Y., Szczygielski, M., Kabacik, L., and Offer, G. J., 2015. "Lithium sulfur battery nail penetration test under load". *Journal of Energy Storage*, 2, pp. 25–29.
- [4] Mikhaylik, Y. V., and Akridge, J. R., 2004. "Polysulfide shuttle study in the li/s battery system". *Journal of The Electrochemical Society*, 151(11), pp. A1969–A1976.
- [5] Bresser, D., Passerini, S., and Scrosati, B., 2013. "Recent progress and remaining challenges in sulfur-based lithium secondary batteries—a review". *Chemical communications*, 49(90), pp. 10545–10562.
- [6] Manthiram, A., Fu, Y., Chung, S.-H., Zu, C., and Su, Y.-S., 2014. "Rechargeable lithium–sulfur batteries". *Chemical reviews*, 114(23), pp. 11751–11787.
- [7] Song, M.-K., Cairns, E. J., and Zhang, Y., 2013.

“Lithium/sulfur batteries with high specific energy: old challenges and new opportunities”. *Nanoscale*, **5**(6), pp. 2186–2204.

[8] Rezan, D.-c., 2017. *Li-S Batteries: The Challenges, Chemistry, Materials, and Future Perspectives*. # N/A.

[9] Kolosnitsyn, V., Kuzmina, E., Karaseva, E., and Mochalov, S., 2011. “A study of the electrochemical processes in lithium–sulphur cells by impedance spectroscopy”. *Journal of Power Sources*, **196**(3), pp. 1478–1482.

[10] Deng, Z., Zhang, Z., Lai, Y., Liu, J., Li, J., and Liu, Y., 2013. “Electrochemical impedance spectroscopy study of a lithium/sulfur battery: modeling and analysis of capacity fading”. *Journal of The Electrochemical Society*, **160**(4), pp. A553–A558.

[11] Knap, V., Stroe, D.-I., Teodorescu, R., Swierczynski, M., and Stanciu, T., 2015. “Electrical circuit models for performance modeling of lithium-sulfur batteries”. In 2015 IEEE Energy Conversion Congress and Exposition (ECCE), IEEE, pp. 1375–1381.

[12] Propp, K., Marinescu, M., Auger, D. J., O’Neill, L., Fotouhi, A., Somasundaram, K., Offer, G. J., Minton, G., Longo, S., Wild, M., et al., 2016. “Multi-temperature state-dependent equivalent circuit discharge model for lithium-sulfur batteries”. *Journal of Power Sources*, **328**, pp. 289–299.

[13] Fotouhi, A., Auger, D. J., Propp, K., Longo, S., Purkayastha, R., O’Neill, L., and Waluś, S., 2017. “Lithium–sulfur cell equivalent circuit network model parameterization and sensitivity analysis”. *IEEE Transactions on Vehicular Technology*, **66**(9), pp. 7711–7721.

[14] Fotouhi, A., Auger, D. J., Propp, K., and Longo, S., 2017. “Lithium–sulfur battery state-of-charge observability analysis and estimation”. *IEEE Transactions on Power Electronics*, **33**(7), pp. 5847–5859.

[15] Propp, K., Auger, D. J., Fotouhi, A., Marinescu, M., Knap, V., and Longo, S., 2019. “Improved state of charge estimation for lithium-sulfur batteries”. *Journal of Energy Storage*, **26**, p. 100943.

[16] Kumaresan, K., Mikhaylik, Y., and White, R. E., 2008. “A mathematical model for a lithium–sulfur cell”. *Journal of The Electrochemical Society*, **155**(8), pp. A576–A582.

[17] Fronczek, D. N., and Bessler, W. G., 2013. “Insight into lithium–sulfur batteries: Elementary kinetic modeling and impedance simulation”. *Journal of power sources*, **244**, pp. 183–188.

[18] Hofmann, A. F., Fronczek, D. N., and Bessler, W. G., 2014. “Mechanistic modeling of polysulfide shuttle and capacity loss in lithium–sulfur batteries”. *Journal of Power Sources*, **259**, pp. 300–310.

[19] Ren, Y., Zhao, T., Liu, M., Tan, P., and Zeng, Y., 2016. “Modeling of lithium-sulfur batteries incorporating the effect of li₂s precipitation”. *Journal of Power Sources*, **336**, pp. 115–125.

[20] Andrei, P., Shen, C., and Zheng, J. P., 2018. “Theoretical and experimental analysis of precipitation and solubility effects in lithium-sulfur batteries”. *Electrochimica Acta*, **284**, pp. 469–484.

[21] Danner, T., and Latz, A., 2019. “On the influence of nucleation and growth of s₈ and li₂s in lithium-sulfur batteries”. *Electrochimica Acta*, **322**, p. 134719.

[22] Marinescu, M., Zhang, T., and Offer, G. J., 2016. “A zero dimensional model of lithium–sulfur batteries during charge and discharge”. *Physical Chemistry Chemical Physics*, **18**(1), pp. 584–593.

[23] Zhang, T., Marinescu, M., O’Neill, L., Wild, M., and Offer, G., 2015. “Modeling the voltage loss mechanisms in lithium–sulfur cells: the importance of electrolyte resistance and precipitation kinetics”. *Physical Chemistry Chemical Physics*, **17**(35), pp. 22581–22586.

[24] Wild, M., O’neill, L., Zhang, T., Purkayastha, R., Minton, G., Marinescu, M., and Offer, G., 2015. “Lithium sulfur batteries, a mechanistic review”. *Energy & Environmental Science*, **8**(12), pp. 3477–3494.

[25] Danner, T., Zhu, G., Hofmann, A. F., and Latz, A., 2015. “Modeling of nano-structured cathodes for improved lithium-sulfur batteries”. *Electrochimica Acta*, **184**, pp. 124–133.

[26] Doosthosseini, M., Hansen, E., and Fathy, H. K., 2019. “On the accuracy of drug-resistant cell population estimation from total cancer size measurements”. In 2019 18th European Control Conference (ECC), IEEE, pp. 343–350.

[27] Ghaznavi, M., and Chen, P., 2014. “Sensitivity analysis of a mathematical model of lithium–sulfur cells part i: Applied discharge current and cathode conductivity”. *Journal of power sources*, **257**, pp. 394–401.

[28] M. Ghaznavi and P. Chen,, 2014. “Sensitivity analysis of a mathematical model of lithium–sulfur cells: Part ii: Precipitation reaction kinetics and sulfur content”. *Journal of Power Sources*, **257**, pp. 402–411.

[29] Ghaznavi, M., and Chen, P., 2014. “Analysis of a mathematical model of lithium-sulfur cells part iii: Electrochemical reaction kinetics, transport properties and charging”. *Electrochimica Acta*, **137**, pp. 575–585.

[30] Li, G., Gao, Y., He, X., Huang, Q., Chen, S., Kim, S. H., and Wang, D., 2017. “Organosulfide-plasticized solid-electrolyte interphase layer enables stable lithium metal anodes for long-cycle lithium-sulfur batteries”. *Nature communications*, **8**, p. 850.

[31] Kennedy, J., and Eberhart, R., 1995. “Particle swarm optimization (pso)”. In Proc. IEEE International Conference on Neural Networks, Perth, Australia, pp. 1942–1948.